MHD disc winds can reproduce fast disc dispersal and the correlation between accretion rate and disc mass in Lupus

Tabone, B.X.J.A.; Rosotti, G.P.; Lodato, G.; Armitage, P.J.; Cridland, A.J.; Dishoeck, E.F. van

Monthly Notices of the ROYAL ASTRONOMICAL SOCIETY

MNRAS **512,** L74–L79 (2022) https://doi.org/10.1093/mnrasl/slab124
Advance Access publication 2021 December 2

MHD disc winds can reproduce fast disc dispersal and the correlation between accretion rate and disc mass in Lupus

B. Tabone [1]★ G. P. Rosotti [1,2] G. Lodato [3] P. J. Armitage,[4,5] A. J. Cridland[6] and E. F. van Dishoeck[1,6]

[1]*Leiden Observatory, Leiden University, PO Box 9513, NL-2300 RA Leiden, the Netherlands*
[2]*School of Physics and Astronomy, University of Leicester, Leicester LE1 7RH, UK*
[3]*Dipartimento di Fisica, Università degli Studi di Milano, Via Celoria 16, I-20133 Milano, Italy*
[4]*Department of Physics and Astronomy, Stony Brook University, Stony Brook, NY 11794, USA*
[5]*Center for Computational Astrophysics, Flatiron Institute, New York, NY 10010, USA*
[6]*Max-Planck-Institut für Extraterrestrische Physik, Giessenbachstrasse 1, D-85748 Garching bei München, Germany*

Accepted 2021 November 26. Received 2021 November 26; in original form 2021 August 4

ABSTRACT

The final architecture of planetary systems depends on the extraction of angular momentum and mass-loss processes of the discs in which they form. Theoretical studies proposed that magnetohydrodynamic winds launched from the discs (MHD disc winds) could govern accretion and disc dispersal. In this work, we revisit the observed disc demographics in the framework of MHD disc winds, combining analytical solutions of disc evolution and a disc population synthesis approach. We show that MHD disc winds alone can account for both disc dispersal and accretion properties. The decline of disc fraction over time is reproduced by assuming that the initial accretion time-scale (a generalization of the viscous time-scale) varies from disc to disc and that the decline of the magnetic field strength is slower than that of the gas. The correlation between accretion rate and disc mass, and the dispersion of the data around the mean trend as observed in Lupus, is then naturally reproduced. The model also accounts for the rapidity of the disc dispersal. This paves the way for planet formation models in the paradigm of wind-driven accretion.

Key words: accretion, accretion discs – MHD – planets and satellites: formation – protoplanetary discs – submillimetre: planetary systems.

1 INTRODUCTION

Unveiling the physical processes that regulate disc evolution is crucial to understand the emergence of the diversity and the habitability of exoplanets (Morbidelli & Raymond 2016). Extensive surveys from the ultraviolet (UV) to the millimetre have shown two essential features of disc evolution: (i) discs, as identified from their infrared (IR) excess, are accreting, implying a transport of angular momentum, and (ii) discs are dispersed after a few Myr in a short time-scale ($\simeq$0.5 Myr).

Over the past decades, these two observational facts have been explained by two distinct processes in the 'paradigm of viscous discs' (Shakura & Sunyaev 1973; Lynden-Bell & Pringle 1974). On the one hand, the magnetorotational instability (MRI), or perhaps other hydrodynamical instabilities, would act as a viscosity, transporting the angular momentum in the radial direction (Armitage 2011, and references therein). On the other hand, UV photons or X-rays would launch hydrodynamical winds, also known as photoevaporative winds, that would quickly disperse the disc (Alexander et al. 2014).

The new generation of telescopes revolutionized our view on disc evolution thanks to complete surveys of star-forming regions. The Atacama Large Millimeter/submillimeter Array (ALMA) has provided continuum fluxes, a proxy for disc masses (e.g. Ansdell et al. 2016; Pascucci et al. 2016), and the Very Large Telescope (VLT) XShooter instrument has measured stellar properties and accretion rates (e.g. Alcalá et al. 2017; Manara et al. 2020). Combining these surveys, Manara et al. (2016) and Mulders et al. (2017) found a correlation between accretion rate and disc mass in Lupus and Chamaeleon with a nearly linear relationship. Whereas such a correlation is expected in viscous models (Hartmann et al. 1998; Rosotti et al. 2017), the large scatter in the relation is in tension with viscous evolution. Lodato et al. (2017) explained this scatter by assuming long viscous time-scales and a dispersion in disc ages but underpredict it in the older region of Upper Scorpius (Manara et al. 2020). Sellek, Booth & Clarke (2020) invoked fast dust radial drift to increase the scatter, but this scenario is in tension with disc sizes measured from dust emission (Toci et al. 2021).

Today, the paradigm of viscous disc evolution is challenged. ALMA observations suggest that at least at large radius (>20 au), turbulence levels are too low to sustain disc accretion (Pinte et al. 2016; Flaherty et al. 2018). Recent numerical simulations further demonstrate that MRI turbulence is quenched in the low-ionization regions of discs called dead zones, where most of the planets are forming ($\gtrsim$1 au; Gammie 1996; Bai & Stone 2011). Following the pioneering work by Blandford & Payne (1982), the emerging paradigm proposes that efficient disc accretion is driven by magnetohydrodynamic winds launched from the disc surface along magnetic field lines (MHD disc winds; Ferreira 1997; Bai & Stone 2013). If disc accretion is driven by an MHD disc wind, every step of planet formation would be impacted. Yet, the majority of planet formation

★ E-mail: benoit.tabone@universite-paris-saclay.fr

models rely on viscous disc models as disc demographics have almost exclusively been analysed in this framework.

In this letter, we use a disc population synthesis approach based on a simple disc evolution model presented in a companion paper (Tabone et al. 2022, hereafter T22) to reconsider the observed disc demographics in the framework of MHD disc winds. The model and the observational data set are presented in Section 2 and the comparison of the model with disc dispersal and accretion properties are detailed in Section 3. Our findings are summarized and discussed in Section 4.

2 METHOD

2.1 Disc population synthesis

The evolution of an ensemble of discs is computed from a disc evolution model presented in T22. In short, the disc is treated in a one-dimensional approach by vertically averaging disc quantities. An MHD disc wind transporting angular momentum and mass is launched from the full extent of the disc. The wind torque and the mass-loss rate are parametrized using a generalization of the α Shakura–Sunyaev parameter, denoted as $\alpha_{\rm DW}$, and the magnetic lever arm parameter, denoted as λ. The correspondence between $\alpha_{\rm DW}$ and other parametrizations of the wind torque (e.g. Suzuki et al. 2016) can be found in T22. In this work, we neglect the viscous torque; i.e. we test the hypothesis that MHD winds alone can account for disc evolution and dispersal. Further assuming that $\alpha_{\rm DW}$ and λ are constant across the disc, analytical solutions for the evolution of a disc with a surface density profile of

$$\Sigma(r,t) = \Sigma_{\rm c}(t)\,(r/r_{\rm c})^{-1+\xi}\,{\rm e}^{-r/r_{\rm c}} \tag{1}$$

are found, where $\Sigma_{\rm c}(t)$ is a characteristic surface density, $\xi = 1/[2(\lambda-1)]$ is the mass ejection index, and $r_{\rm c}$ is the disc characteristic size. In the absence of viscosity, $r_{\rm c}$ is constant in time as no angular momentum is radially transported. The disc extends down to an inner radius $r_{\rm in}$. In order to describe discs that disperse at a finite time, we used the $\Sigma_{\rm c}$-dependent wind torque solutions of T22, for which $\alpha_{\rm DW}$ increases (implicitly) with time as

$$\alpha_{\rm DW}(t) = \alpha_{\rm DW}(0)\,(\Sigma_{\rm c}(t)/\Sigma_{\rm c}(0))^{-\omega}\,, \tag{2}$$

where ω is a phenomenological parameter between 0 and 1 that quantifies the (unknown) dissipation of the magnetic field. For $\omega = 1$, the magnetic field strength in the disc is constant.

In this paper, we focus on the evolution of the disc mass $M_{\rm D}(t)$ and the stellar accretion rate $\dot{M}_*(t)$ that read

$$\begin{aligned} M_{\rm D}(t) &= M_0\left(1-\frac{\omega}{2t_{\rm acc,0}}t\right)^{1/\omega}\,,\\ \dot{M}_*(t) &= \frac{M_0}{2t_{\rm acc,0}(1+f_M)}\left(1-\frac{\omega}{2t_{\rm acc,0}}t\right)^{-1+1/\omega}\,, \end{aligned} \tag{3}$$

where

$$f_M \equiv \dot{M}_W/\dot{M}_* = (r_{\rm c}/r_{\rm in})^{\xi} - 1 \tag{4}$$

is the mass ejection-to-accretion ratio, and

$$t_{\rm acc,0} \equiv \frac{r_{\rm c}}{3\epsilon_{\rm c}c_{\rm s,c}\alpha_{\rm DW}(0)} \tag{5}$$

is the initial accretion time-scale that is a generalization of the viscous time-scale, where $\epsilon_{\rm c}$ is the disc aspect ratio and $c_{\rm s,c}$ is the sound speed at $r = r_{\rm c}$. Therefore, $M_{\rm D}(t)$ and $\dot{M}_*(t)$ are controlled by four independent parameters: M_0, f_M, $t_{\rm acc,0}$, and ω. The time evolution of the solutions is shown in Fig. 1 and discussed below. Throughout this letter, the initial time corresponds to the end of the Class I stage when the infall rate is much smaller than the disc accretion rate.

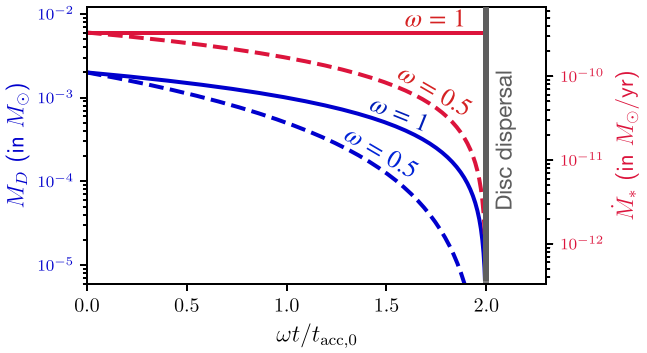

Figure 1. Evolution of the disc mass (in blue) and accretion rate (in red) for two values of the ω parameter. The accretion time-scale is $t_{\rm acc,0} = 1$ Myr, the initial disc mass is $M_0 = 2 \times 10^{-3}$ M$_\odot$, and $f_M = 2$. For $\omega > 0$, the disc is fully dispersed at a finite time $t_{\rm disp}$ (see equation 6). ω describes the time evolution of the magnetic field strength. High values of ω correspond to disc magnetic fields that decline more slowly, resulting in a shallower decline of the disc mass and accretion rate before dispersal.

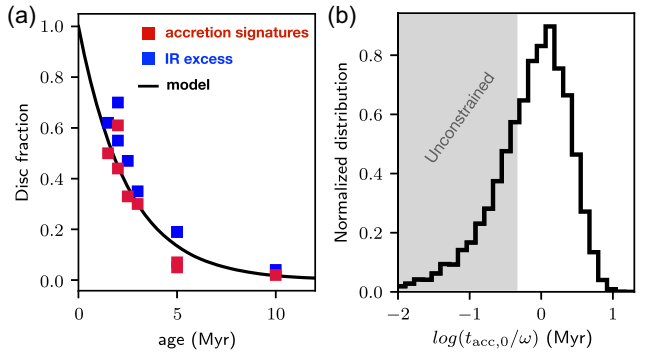

Figure 2. Distribution of initial accretion time-scale $t_{\rm acc,0}$ inferred from disc dispersal. (a) Fraction of sources with IR excess and accretion signatures towards star-forming regions from Fedele et al. (2010), and the fit adopted in this study. (b) Inferred distribution of $t_{\rm acc,0}$. The x-axis is normalized by $t_{\rm acc,0}/\omega$ such that the plotted distribution does not depend on ω.

From this simplified disc evolution model, we build a disc population model by randomly selecting initial disc mass M_0 and accretion time-scale $t_{\rm acc,0}$ and computing the evolution of the population. For the sake of conciseness, for each synthetic population, ω and f_M are fixed. The distribution of $t_{\rm acc,0}$ is fitted from the observed disc fraction as detailed in Section 3.1. The initial disc mass M_0 follows a lognormal distribution with a dispersion of 1 dex. A dispersion in the predicted accretion rates of 0.45 dex is added to account for short-term accretion variability as in Lodato et al. (2017).

2.2 Observational data

The fractions of disc-bearing sources towards star-forming regions of different ages stem from the compilation by Fedele et al. (2010) (see Fig. 2a). New extensive ALMA and XShooter surveys open the possibility of accurately testing disc evolution models. In this work, disc masses and accretion rates in the Lupus star-forming region, where external photoevaporation is minimal, are collected from the compilation of Manara et al. (2019), who used distances from the

Gaia Data Release 2 (Gaia Collaboration 2018). The total disc masses (gas and dust) are estimated from dust continuum emission observed by ALMA (Ansdell et al. 2016) by assuming a gas-to-dust ratio of 100, optically thin emission, a dust temperature of 20 K, and a dust opacity of 2.3 $cm^2\ g^{-1}$ (ν/230 GHz). The data set includes the young stellar objects (YSOs) in Lupus I–IV with stellar mass above $M_* > 0.1\ M_\odot$ with a completeness rate of 96 per cent. The accretion rates of the same sample are from a VLT-XShooter survey analysed by Alcalá et al. (2014, 2017).

3 RESULTS

3.1 Disc dispersal

Extensive surveys show that the fraction of sources with IR excess or accretion signatures drops with the cluster age over a typical time of about 2–3 Myr (see Fig. 2a). Our disc evolution model predicts that a disc is fully dispersed after (see Fig. 1)

$$t_{\rm disp} = 2t_{\rm acc,0}/\omega. \quad (6)$$

We shall insist here that disc dispersal is not a result of the mass lost in the wind, but of the absence of disc spreading and of the increase in $\alpha_{\rm DW}$ over time. Indeed, the disc dispersal time $t_{\rm disp}$ does not depend on the value of f_M, i.e. the fraction of mass ejected in the wind compared to that accreted onto the star. Following equation (6), the decline of disc fraction with age can be interpreted as the result of a distribution of the initial accretion time-scale $t_{\rm acc,0}$. For example, the fact that 30 per cent of YSOs bear a disc in the 3 Myr-old σ-Ori cluster points towards a population that had initially 30 per cent of its discs born with $t_{\rm disp} > 3$ Myr. Following this approach, we assume that all the clusters studied by Fedele et al. (2010) had initially the same distribution of $t_{\rm acc,0}$ (or equivalently, $t_{\rm disp}$). We further assume that the transition between 'disc-bearing' (Class II) and 'disc-less' (Class III) stage occurs at $t = t_{\rm disp}$. The initial distribution of $t_{\rm acc,0}$ required to fit the disc frequency with cluster age can then be derived from the fraction of disc-bearing sources denoted as $f_{\rm D}$ (see supplementary material). One of the complications is that $f_{\rm D}$ depends on the criterion used to measure the fraction of Class II sources. The dispersal time obtained from accretion signatures is shorter (2.3 Myr) than that of the inner disc traced by IR wavelengths (3 Myr). This effect might be the result of dust evolution and/or a difference between the sensitivity of the two diagnostics. We adopt here a characteristic disc dispersal time (τ) of 2.5 Myr and a disc fraction of $f_{\rm D}(t) = {\rm e}^{-t/\tau}$.

The resulting distribution of $t_{\rm acc,0}$ is shown in Fig. 2(b). The majority of discs are born with $t_{\rm acc,0}$ of about $1.5/\omega$ Myr, which is, by construction, about half the disc dispersal time τ. Because disc fraction is typically measured for clusters older than $\simeq$1 Myr, the distribution for short values of $t_{\rm acc,0}$ ($\lesssim 0.5/\omega$ Myr) is poorly constrained. However, discs born with these short values of $t_{\rm acc,0}$ are quickly dispersed and do not affect our predictions for ages above $\simeq$1 Myr. In the following, all the synthetic populations follow the distribution of $t_{\rm acc,0}$ shown in Fig. 2(b) such that the fraction of disc-bearing sources in the synthetic populations always reproduces that observed.

3.2 Correlation between accretion rate and disc mass

In this section, we show that given the distribution of $t_{\rm acc,0}$ inferred from the disc fraction, the accretion properties observed in Lupus are naturally reproduced. We first adopt $\omega = 1$, which corresponds to discs of constant magnetic field strength. The only parameters that are left free are the distribution of initial disc masses M_0, and the value of f_M. In the model, the evolution of disc mass depends only on $t_{\rm acc,0}$ [see equation (3) and supplementary material]. For $\omega = 1$, the median mass of the synthetic population decreases by a factor of 3 in 2 Myr. In order to reproduce the median disc mass inferred in Lupus, an initial median disc mass of $2 \times 10^{-3}\ M_\odot$ is then adopted.

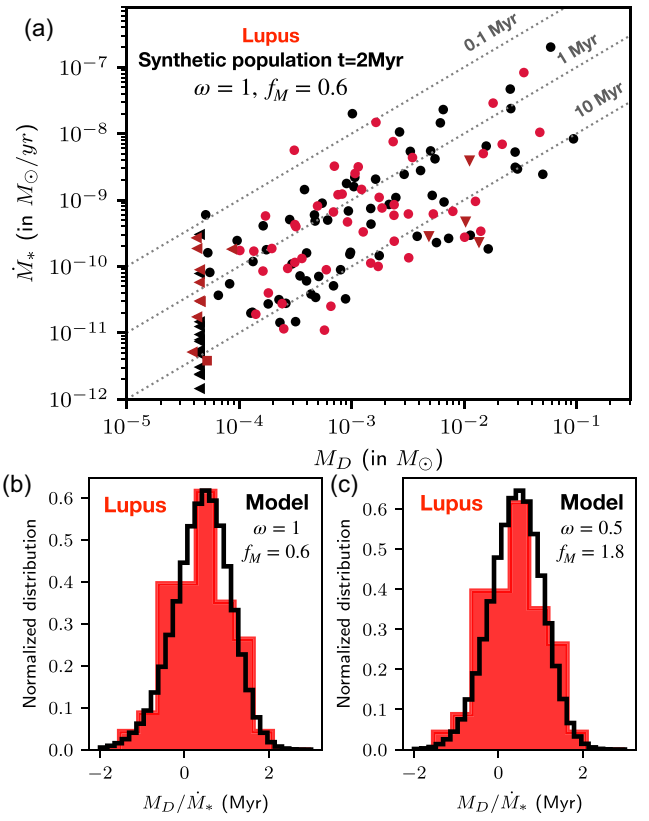

Figure 3. Correlation between accretion rate and disc mass. (a) Location of the discs in the $\dot{M}_*$–$M_{\rm D}$ plane after 2 Myr for a synthetic population with $\omega = 1$ and $f_M = 0.6$ (black), and the Lupus disc population (red). (b) The corresponding distribution of the disc lifetime $t_{\rm lt} = M_{\rm D}/\dot{M}_*$. In order to avoid statistical fluctuation, a sample of 10^6 discs has been computed. Synthetic discs with a mass below the detection threshold of the ALMA survey are excluded. (c) Same as panel (b) but for $\omega = 0.5$ and $f_M = 1.8$.

We then follow the evolution of 200 discs, of which 90 have survived at the age of Lupus, in line with the disc fraction estimated in this cluster. Fig. 3(a) compares the accretion properties of a synthetic population after 2 Myr for $f_M = 0.6$ with the Lupus sample in the $\dot{M}_*$–$M_{\rm D}$ plane. The model reproduces remarkably well the clustering of the data. We stress that the model has been constructed to reproduce disc fractions and the median disc mass. We have made no adjustment to reproduce the accretion rate distribution nor the dispersion in the data, so this is a significant achievement of the model. We recover the nearly linear relationship between accretion rates and disc masses found in the Lupus and Chamaeleon regions (Manara et al. 2016; Mulders et al. 2017). Therefore, this correlation is not a distinctive feature of viscous evolution. In fact, the correlation found in our wind model is a consequence of the assumption that the distribution of $t_{\rm acc,0}$ is independent of M_0. The latter assumption amounts to assume that discs of different masses are born with a similar distribution of magnetization and size. It remains to be determined by future work how much correlation between $t_{\rm acc,0}$ and M_0 can be introduced to remain consistent with the data.

Even more striking is the agreement with the large dispersion of the data around the mean trend. As explained below, the predicted dispersion is the result of the dispersion in $t_{\rm acc,0}$, which has been independently derived from the disc fraction. Because $M_{\rm D}$ is on average proportional to $\dot{M}_*$, it is more convenient to investigate the accretion properties using the so-called observed disc lifetime:

$$t_{\rm lt} \equiv M_{\rm D}/\dot{M}_*. \quad (7)$$

Indeed, in our model, $t_{\rm lt}$ does not depend on the initial disc mass M_0 and the only free parameter that affects its value is f_M, $t_{\rm acc,0}$ being set by disc fraction. The distribution of $t_{\rm lt}$ shown in Fig. 3(b) confirms the agreement between the model and the data. The median value of $t_{\rm lt}$ is set by the distribution of $t_{\rm acc,0}$ and the value of f_M. Increasing the ejection-to-accretion mass ratio f_M lowers the accretion rates (equation 3), shifting the distribution of $t_{\rm lt}$ to larger values by a factor $1 + f_M$. In fact, the median disc lifetime of $\simeq$2.7 Myr is recovered for $f_M = 0.6$, a value in line with the mass-loss rates inferred from ALMA observations of MHD disc wind candidates (e.g. Louvet et al. 2018; de Valon et al. 2020; Tabone et al. 2020).

The observed dispersion in $t_{\rm lt}$ of 0.8 dex around the median value is also reproduced, yet somewhat underestimated by the model (0.65 dex). Still, the predicted dispersion is a conservative value since any other processes affecting the estimates of the disc quantities are not included (apart from short-term variability of $\dot{M}_*$). The predicted dispersion in $t_{\rm lt}$ is only set by the dispersion in $t_{\rm acc,0}$, which stems from disc fraction. Therefore, our prediction is robust and suggests that the spread in the $\dot{M}_*$–$M_{\rm D}$ plane, which reflects the extraction of angular momentum, is profoundly connected to disc dispersal time.

Interestingly, we find that the predicted distribution of $t_{\rm lt}$ does not depend on time (see supplementary material). This result is in stark contrast with viscous evolution models that predict a decline of the dispersion and an increase in the median disc lifetime with the age of the cluster (Hartmann et al. 1998; Lodato et al. 2017). The dispersion observed in the older region Upper Sco ($\simeq$6 Myr) could be reproduced by our simple model and dust evolution is not required to account for it, in contrast with viscous models (Sellek et al. 2020). However, the comparison with Upper Sco is beyond the scope of this paper as dust evolution might still affect the gas-to-dust ratio and so the median value of $t_{\rm lt}$.

We now explore a more generic case of $\omega < 1$ to demonstrate that there is no requirement in the model to fine-tune ω. For a smaller value of ω, the disc mass and accretion rate of an individual disc experience a steeper drop before being dispersed (see Fig. 1). For $\omega = 0.5$, we adopt a median disc mass of 4×10^{-3} M$_\odot$ to reproduce that observed in Lupus. Interestingly, this value is more in line with the median mass of Class I discs than in the case $\omega = 1$ (when assuming a similar dust opacity coefficient as in Lupus; see Tobin et al. 2020; Tychoniec et al. 2020). As in the case $\omega = 1$, the nearly linear relationship between $M_{\rm D}$ and $\dot{M}_*$ is recovered. The median disc lifetime is well reproduced for $f_M = 1.8$ (Fig. 3c), a value that is higher than that in the case $\omega = 1$. In fact, for lower values of ω, the accretion time-scale $t_{\rm acc,0}$ required to fit disc dispersal is reduced by a factor of ω (Fig. 2b). Since $\dot{M}_* \propto t_{\rm acc,0}^{-1}$ (equation 3), lower values of ω lead to higher values of $\dot{M}_*$. In order to remain compatible with the observed median disc lifetime $M_{\rm D}/\dot{M}_*$, a higher value of f_M is required.

At this stage, any value of ω seems to reproduce the data. However, for $\omega < 0.5$, our criterion that the transition between Class II and Class III stage corresponds to $t = t_{\rm disp}$ fails. In fact, for these low values of ω, disc masses and accretion rates smoothly drop below the detection limits of the surveys before $t = t_{\rm disp}$. In that case, our simplified approach provides a lower limit on $t_{\rm acc,0}$. A more sophisticated analysis of detection thresholds, which is beyond the scope of this paper, has to be carried out.

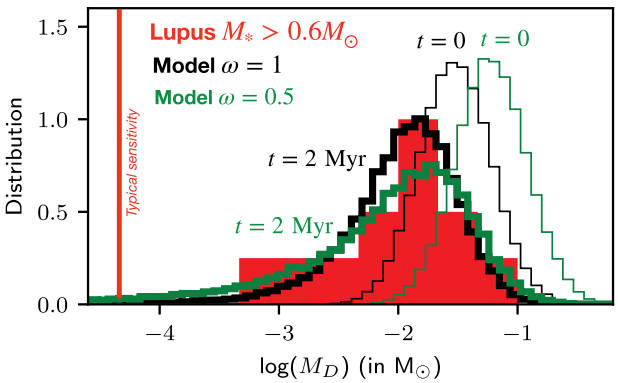

Figure 4. Rapidity of disc dispersal as probed by the distribution of $M_{\rm D}$ for stellar masses above 0.6 M$_\odot$ inferred in Lupus (in red) compared to that predicted by our synthetic population for $\omega = 1$ and 0.5 (in black and green thick lines, respectively). The initial distributions of disc mass for the two models are in thin lines. The scarcity of disc masses in the range of 3×10^{-5}–10^{-3} M$_\odot$ demonstrates that our model reproduces the rapidity of the disc dispersal.

3.3 Rapidity of the disc dispersal

Disc dispersal is a fast process: After a few Myr, the disc is quickly dispersed within $\lesssim$0.5 Myr. In this section, we show that without any further adjustment of $t_{\rm acc,0}$ or f_M, the rapidity of disc dispersal is reproduced. To do so, we focus on the discs around the most massive stars, because only in this case is the observational mass sensitivity enough to detect all the Class II discs (Lovell et al. 2021).

Fig. 4 (red histogram) shows that discs observed in Lupus around stars more massive than 0.6 M$_\odot$ are confined to high mass, typically above $M_{\rm D} \simeq 10^{-3}$ M$_\odot$, and far above the detection threshold of the survey. This can be interpreted as the footprint of a rapid dispersal of the disc: Prior to its full dispersal, a disc runs along the x-axis of Fig. 4 as its mass drops. If discs were to disperse slowly, they would have been distributed all the way down to the detection threshold, which is not what is observed.

To compare our model to this subsample, we ran a synthetic population that describes discs around the most massive stars by increasing the initial median disc mass to $3 \times 10^{-2}/\omega$ M$_\odot$ to reproduce that observed around stars with $M_* \geq 0.6$ M$_\odot$. An initial dispersion of 0.3 dex is also adopted to reproduce the observed spread in $M_{\rm D}$. This is lower than the dispersion adopted to reproduce the full Lupus sample. In fact, in the latter, the high dispersion in $M_{\rm D}$ is driven by the distribution of stellar mass of the sample in virtue of the correlation between the stellar and disc masses (Pascucci et al. 2016).

Fig. 4 shows the predicted distribution of $M_{\rm D}$ at $t = 0$ and at the age of Lupus. For the case $\omega = 1$ (black histograms), while the distribution of disc masses is initially symmetric (see thin lines), by the age of Lupus the distribution has acquired a tail at low disc masses, corresponding to discs that are being dispersed. Overall, the distribution of disc mass is remarkably well reproduced. In particular, the scarcity of discs around 10^{-4} M$_\odot$ is recovered. This demonstrates that the dispersal process predicted by our MHD wind model is fast enough. For lower values of ω, the tail is somewhat more pronounced (see thick green histogram) as the mass of an individual disc declines more slowly prior to the full dispersal (see Fig. 1). Still the model

with $\omega = 0.5$ reproduces well the data. For even lower values of ω, the model is in tension with the data as the occurrence of low-mass discs increases. However, as mentioned earlier, more sophisticated models have to be built to explore this parameter space.

4 CONCLUDING REMARKS

In this work, we show that the essential features of disc evolution as probed by the observations are naturally reproduced by MHD wind-driven accretion. Starting with an initial distribution of accretion time-scale $t_{\rm acc,0}$, the frequency of disc-bearing sources with time is reproduced. Given this distribution and without further adjustment, the accretion properties of discs, as characterized by the correlation between accretion rate and disc mass, and the dispersion of the data around the mean trend, are naturally reproduced. A wind mass-loss rate of about the accretion rate ($f_M \simeq 1$) is required to reproduce the median $M_{\rm D}/\dot{M}_*$ ratio. Finally, without any additional adjustment, the rapidity of the disc dispersal is accounted for. Therefore, the paradigmatic model of viscous evolution, for which disc accretion is governed by turbulence and dispersal by photoevaporative winds, is not the only scenario that accounts for disc demographics, especially in regions without strong external photoevaporation such as Lupus.

To first order, the distribution of $t_{\rm acc,0}$ can be seen as the result of an underlying distribution of the disc size $r_{\rm c}$ and the initial disc magnetization β_0, i.e. the ratio between the thermal and the magnetic pressure in the mid-plane (see T22, equation 70). Assuming a disc size of $\simeq$50 au, the distribution of $t_{\rm acc,0}$ translates to a typical initial disc magnetization of $\beta_0 \simeq 10^5$ at $r = r_{\rm c}$. Numerical simulations of disc formation (e.g. Hennebelle et al. 2020) running until the late Class I stage are needed to test this prediction and build a complete view of disc evolution, from their formation to their dispersal.

In this work, we estimated the disc gas mass from the (sub)millimetre dust emission assuming a standard gas-to-dust ratio of 100 and standard optical properties (Beckwith et al. 1990). Radial drift makes the dust-to-gas ratio decrease with time so that the gas mass may be underestimated. Modelling of dust coagulation and radial drift (Sanchis et al. 2020) shows, however, that at the age of Lupus the dust masses likely remain better indicators of the total mass than alternative tracers such as CO isotopologues. If disc masses are higher than those derived in this work, the estimated distribution of disc lifetimes $M_{\rm D}/\dot{M}_*$ shown in Figs 3(b) and (c) would be shifted to higher values. Our model would still be able to reproduce the data with higher values of f_M, and higher initial median disc masses. We also note that if winds carry a significant fraction of mass ($f_M \gtrsim 1$), as suggested by this work, they would tend to increase the dust-to-gas ratio as winds are launched from the disc upper layers that are depleted in dust due to dust settling (Miyake, Suzuki & Inutsuka 2016; Giacalone et al. 2019). We plan to study these effects in future papers.

One of the most discriminant features between wind-driven and viscosity-driven accretion is the absence of disc spreading in the former scenario. ALMA surveys of the gas are required to evidence a possible disc viscous spreading (Trapman et al. 2020). A deep systematic search for MHD disc winds launched from the bulk part of the discs has also to be conducted to determine whether the MHD disc wind candidates unveiled in two YSOs, namely HH30 and HD163296, are common (Louvet et al. 2018; Booth et al. 2021). Whereas near-IR and optical lines hint at the ubiquity of such winds (e.g. Pontoppidan, Blake & Smette 2011; Gangi et al. 2020), spatially and spectrally resolved observations, for example with ALMA, are required to infer the mass and angular momentum effectively extracted by the winds (Tabone et al. 2020). Sources with the highest accretion rates, for which MHD disc winds are believed to be rich in CO, should be prime targets (Panoglou et al. 2012; Wang, Bai & Goodman 2019).

All in all, this first study provides us with observationally tested disc evolution models that are required to study dust evolution and planet formation in the emerging paradigm of MHD disc winds.

ACKNOWLEDGEMENTS

The authors thank the anonymous referee for their constructive comments. BT acknowledges support from the research programme Dutch Astrochemistry Network II with project number 614.001.751, which is (partly) financed by the Dutch Research Council (NWO). GR acknowledges support from the Netherlands Organisation for Scientific Research (NWO; programme number 016.Veni.192.233) and from an STFC Ernest Rutherford Fellowship (grant number ST/T003855/1). This work is also funded by the Deutsche Forschungsgemeinschaft (DFG, German Research Foundation) - 325594231, FOR 2634/2. We are grateful to C. F. Manara for sharing the Lupus data.

DATA AVAILABILITY

The data underlying this article will be shared on reasonable request to the corresponding author.

REFERENCES

Alcalá J. M. et al., 2014, A&A, 561, A2
Alcalá J. M. et al., 2017, A&A, 600, A20
Alexander R., Pascucci I., Andrews S., Armitage P., Cieza L., 2014, in Beuther H., Klessen R. S., Dullemond C. P., Henning T., eds, Protostars and Planets VI. Univ. Arizona Press, Tucson, AZ, p. 475
Ansdell M. et al., 2016, ApJ, 828, 46
Armitage P. J., 2011, ARA&A, 49, 195
Bai X.-N., Stone J. M., 2011, ApJ, 736, 144
Bai X.-N., Stone J. M., 2013, ApJ, 769, 76
Beckwith S. V. W., Sargent A. I., Chini R. S., Guesten R., 1990, AJ, 99, 924
Blandford R. D., Payne D. G., 1982, MNRAS, 199, 883
Booth A. S. et al., 2021, ApJS, 257, 16
de Valon A., Dougados C., Cabrit S., Louvet F., Zapata L. A., Mardones D., 2020, A&A, 634, L12
Fedele D., van den Ancker M. E., Henning T., Jayawardhana R., Oliveira J. M., 2010, A&A, 510, A72
Ferreira J., 1997, A&A, 319, 340
Flaherty K. M., Hughes A. M., Teague R., Simon J. B., Andrews S. M., Wilner D. J., 2018, ApJ, 856, 117
Gaia Collaboration, 2018, A&A, 616, A1
Gammie C. F., 1996, ApJ, 457, 355
Gangi M. et al., 2020, A&A, 643, A32
Giacalone S., Teitler S., Königl A., Krijt S., Ciesla F. J., 2019, ApJ, 882, 33
Hartmann L., Calvet N., Gullbring E., D'Alessio P., 1998, ApJ, 495, 385
Hennebelle P., Commerçon B., Lee Y.-N., Charnoz S., 2020, A&A, 635, A67
Lodato G., Scardoni C. E., Manara C. F., Testi L., 2017, MNRAS, 472, 4700
Louvet F., Dougados C., Cabrit S., Mardones D., Ménard F., Tabone B., Pinte C., Dent W. R. F., 2018, A&A, 618, A120
Lovell J. B. et al., 2021, MNRAS, 500, 4878
Lynden-Bell D., Pringle J. E., 1974, MNRAS, 168, 603
Manara C. F. et al., 2016, A&A, 591, L3
Manara C. F., Mordasini C., Testi L., Williams J. P., Miotello A., Lodato G., Emsenhuber A., 2019, A&A, 631, L2
Manara C. F. et al., 2020, A&A, 639, A58

Miyake T., Suzuki T. K., Inutsuka S.-i., 2016, ApJ, 821, 3
Morbidelli A., Raymond S. N., 2016, J. Geophys. Res. (Planets), 121, 1962
Mulders G. D., Pascucci I., Manara C. F., Testi L., Herczeg G. J., Henning T., Mohanty S., Lodato G., 2017, ApJ, 847, 31
Panoglou D., Cabrit S., Pineau Des Forêts G., Garcia P. J. V., Ferreira J., Casse F., 2012, A&A, 538, A2
Pascucci I. et al., 2016, ApJ, 831, 125
Pinte C., Dent W. R. F., Ménard F., Hales A., Hill T., Cortes P., de Gregorio-Monsalvo I., 2016, ApJ, 816, 25
Pontoppidan K. M., Blake G. A., Smette A., 2011, ApJ, 733, 84
Rosotti G. P., Clarke C. J., Manara C. F., Facchini S., 2017, MNRAS, 468, 1631
Sanchis E. et al., 2020, A&A, 633, A114
Sellek A. D., Booth R. A., Clarke C. J., 2020, MNRAS, 498, 2845
Shakura N. I., Sunyaev R. A., 1973, A&A, 500, 33
Suzuki T. K., Ogihara M., Morbidelli A., Crida A., Guillot T., 2016, A&A, 596, A74
Tabone B. et al., 2020, A&A, 640, A82
Tabone B., Rosotti G. P., Cridland A. J., Armitage P. J., Lodato G., 2022, MNRAS, in press (T22)
Tobin J. J. et al., 2020, ApJ, 890, 130
Toci C., Rosotti G., Lodato G., Testi L., Trapman L., 2021, MNRAS, 507, 818
Trapman L., Rosotti G., Bosman A. D., Hogerheijde M. R., van Dishoeck E. F., 2020, A&A, 640, A5
Tychoniec Ł. et al., 2020, A&A, 640, A19
Wang L., Bai X.-N., Goodman J., 2019, ApJ, 874, 90

SUPPORTING INFORMATION

Supplementary data are available at *MNRASL* online.

mnras_tabone-SupplMat-clean.pdf

Please note: Oxford University Press is not responsible for the content or functionality of any supporting materials supplied by the authors. Any queries (other than missing material) should be directed to the corresponding author for the article.

This paper has been typeset from a TEX/LATEX file prepared by the author.